From a Dy(III) Mononuclear Single Molecule Magnet (SMM) to a Ferromagnetic [Mn(II)Dy(III)Mn(II)] Trinuclear Complex

Asamanjoy Bhunia,[1] Michael T. Gamer,[1] Liviu Ungur,[2,3] Liviu F. Chibotaru,[2] Annie K. Powell,[1,4*] Yanhua Lan,[1*] Peter W. Roesky,[1*] Fabian Menges,[5] Christoph Riehn,[5] and Gereon Niedner-Schatteburg[5]*

[1]Institut für Anorganische Chemie, Karlsruher Institut für Technologie (KIT), Engesserstr. 15, 76128 Karlsruhe, Germany. [2]Division of Quantum and Physical Chemistry, Katholieke Universiteit Leuven, Celestijenlaan 200F, 3001 Leuven, Belgium. [3]INPAC-Institute of Nanoscale Physics and Chemistry, Katholieke Universiteit Leuven, Celestijenlaan 200F, 3001 Leuven, Belgium. [4]Insitut für Nanotechnologie, Karlsruher Institut für Technologie (KIT), Postach 3640, D-76021 Karlsruhe, Germany. [5]Fachbereich Chemie, Technische Universität Kaiserslautern und Landesforschungszentrum OPTIMAS, Erwin-Schrödinger-Straße, Gebäude 52 67663 Kaiserslautern.

Supporting Information

25 pages

Magnetic data

Mononuclear Dy compound in a pure and diluted (containing 20% Dy) form. See the code indicated in the inset of Figures for discrepancy.

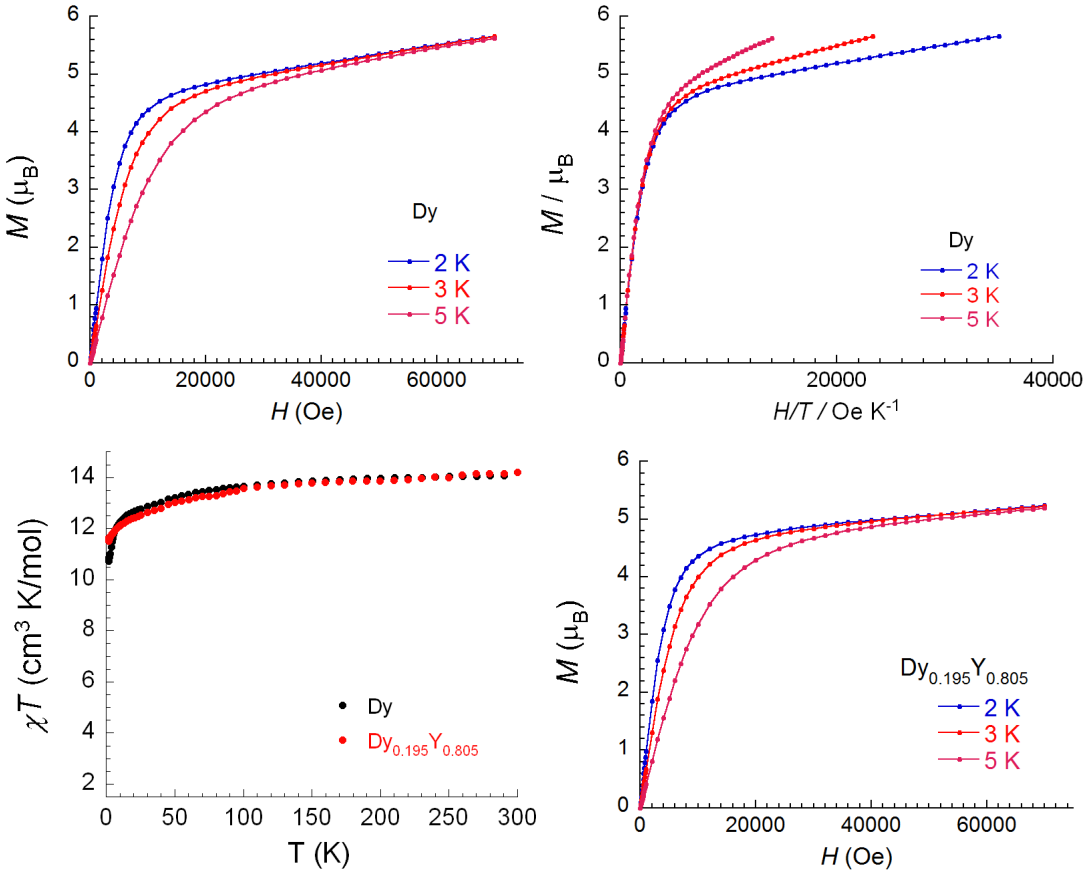

Figure S1: DC magnetic data. Field dependence of magnetization as *M* vs *H* or *M vs H/T* plots; temperature dependence of susceptibility as χT vs T plots.

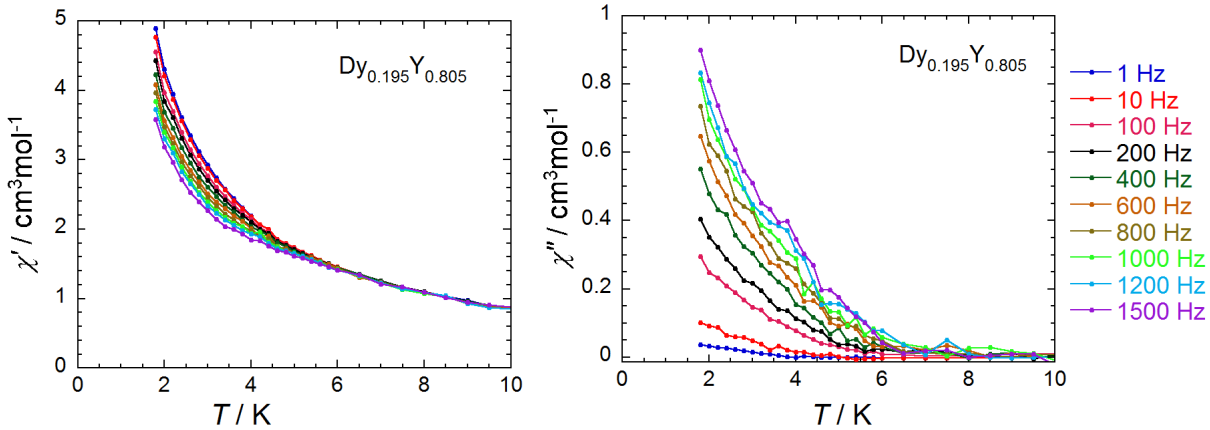

Figure S2: Temperature dependence of the in-phase (left) and the out-of-phase (right) ac susceptibility components at different frequencies.

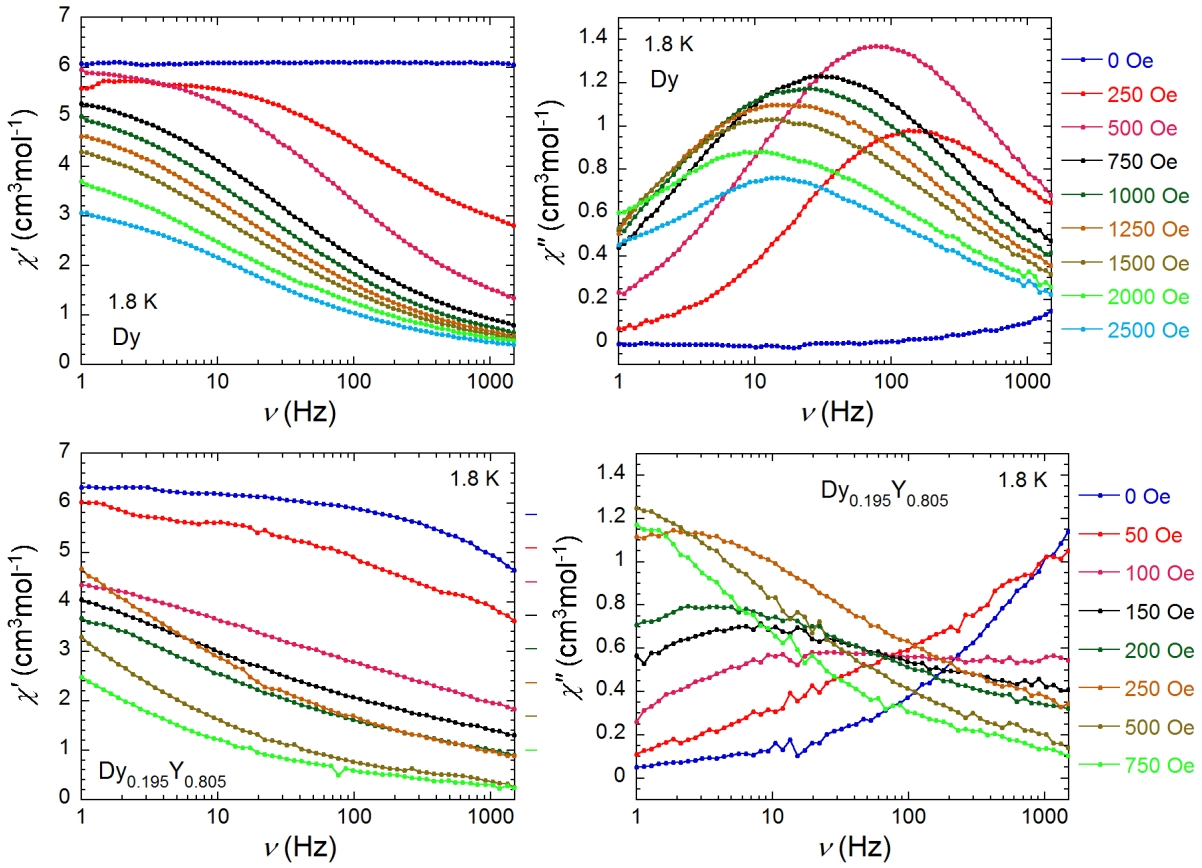

Figure S3. Frequency dependence at 1.8 K of the in-phase (left) and the out-of-phase (right) ac susceptibility components at different dc fields.

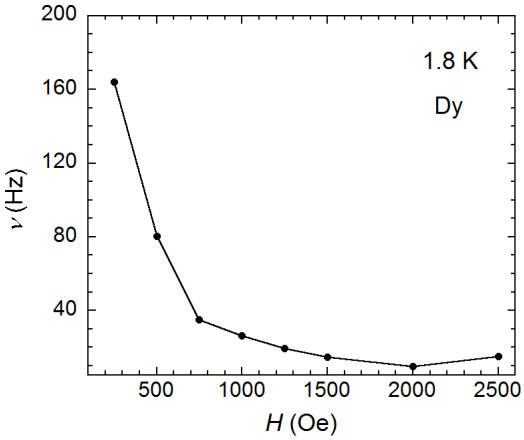

Figure S4. DC field dependence of the frequency at 1.8 K for **1**, the pure compound. The solid line is a guide for the eye.

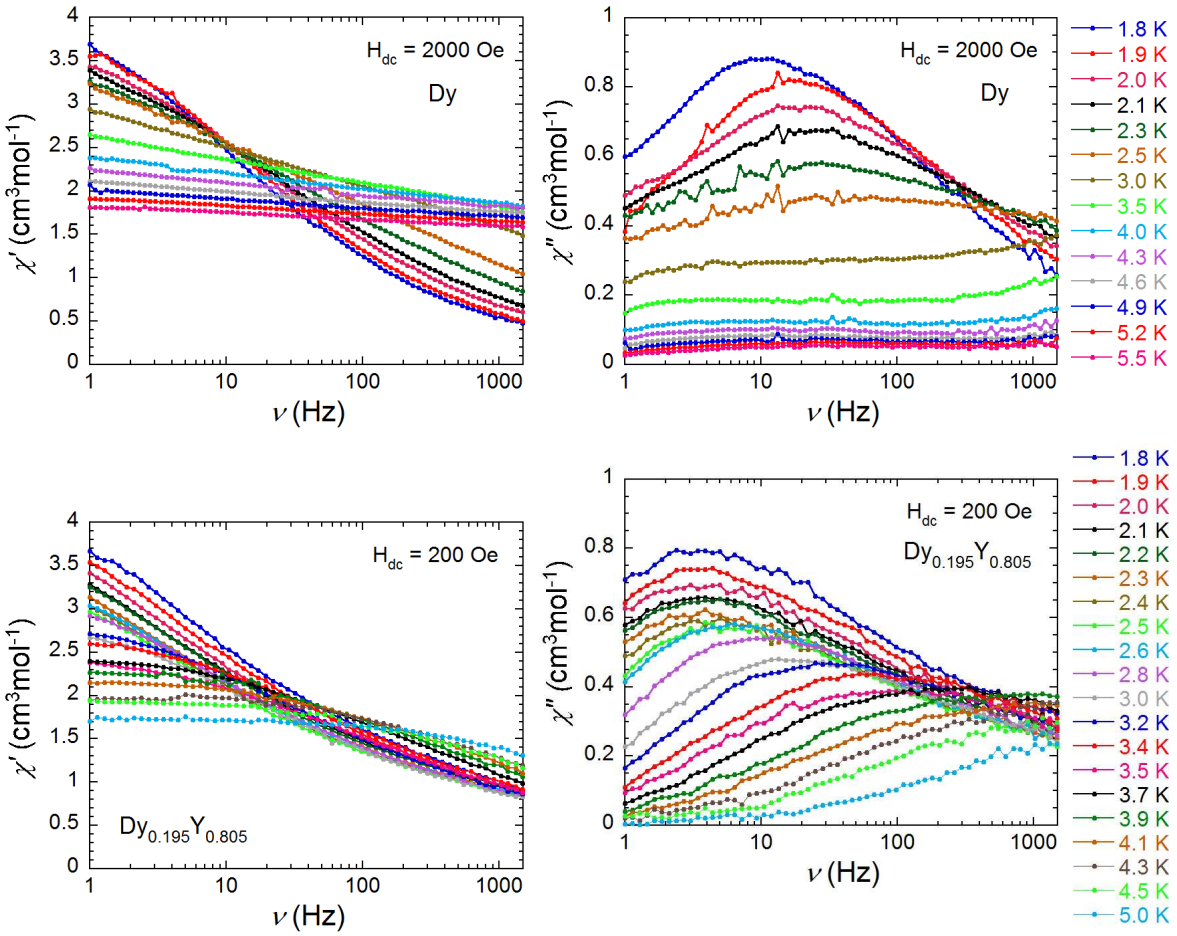

Figure S5. Frequency dependence of the in-phase (left) and the out-of-phase (right) ac susceptibility components under an external DC field as indicated.

a)

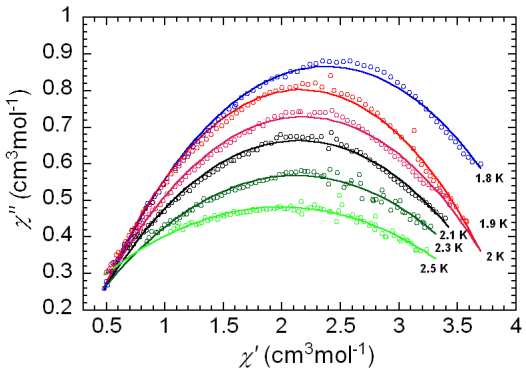

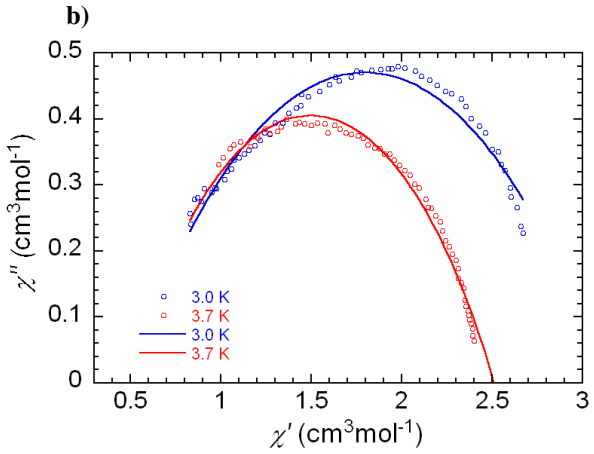

Figure S6. Cole-Cole plots of **1**, the pure (a) and diluted (b) compound at indicated temperatures. The solid lines are the fittings with a generalized Debye model. The parameters (Table S1) are discussed in the text.

Table S1. Parameters obtained from the fits of Cole-Cole diagram in **1**.

T (K)	α	χ_0 (cm^3/mol)	χ_{inf} (cm^3/mol)	R^2
		pure compound		
1.8	0.524(2)	0.168(6)	4.590(14)	0.996
1.9	0.514(3)	0.162(9)	4.161(13)	0.989
2.0	0.570(3)	0.101(9)	4.256(13)	0.992
2.1	0.607(3)	0.054(11)	4.225(15)	0.988
2.3	0.678(4)	0.080(24)	4.324(28)	0.958
2.5	0.748(5)	0.0418(54)	4.404(43)	0.907
		diluted compound		
3.0	0.561(8)	0.486(18)	3.112(23)	0.941
3.2	0.548(8)	0.494(21)	3.022(18)	0.941
3.4	0.531(6)	0.506(17)	2.801(9)	0.978
3.5	0.529(7)	0.469(17)	2.527(8)	0.981
3.7	0.516(8)	0.480(24)	2.512(7)	0.983
3.9	0.548(16)	0.327(72)	2.378(12)	0.959

Mn-Dy-Mn

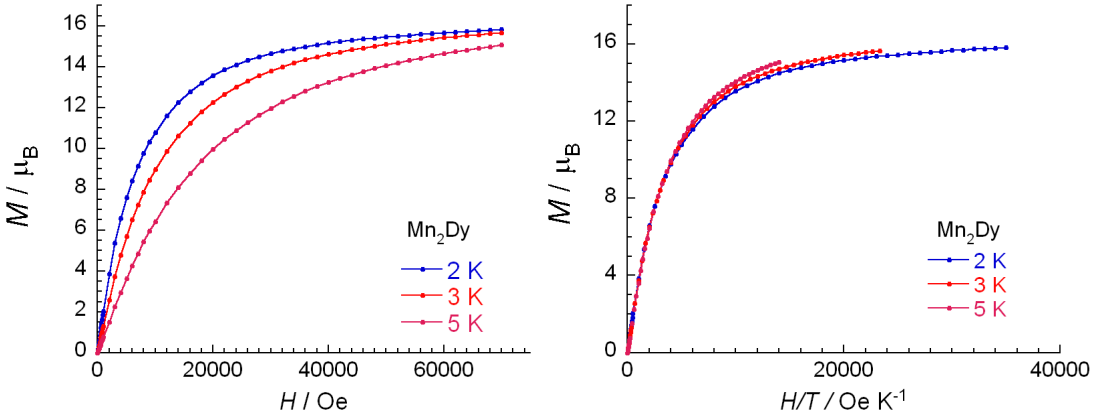

Figure S7: Field dependence of magnetization of **2** as both plots of *M vs H* and *M vs H/T* at indicated temperatures.

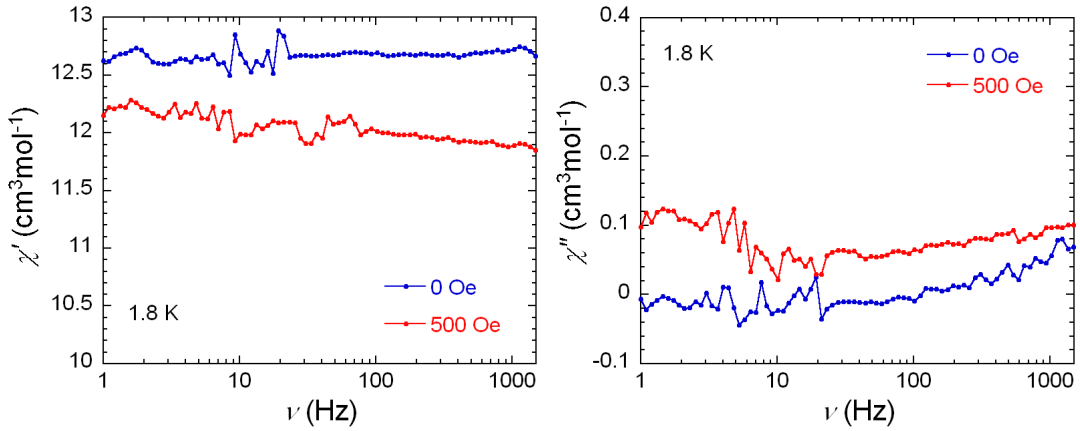

Figure S8. Frequency dependence at 1.8 K of the in-phase (left) and the out-of-phase (right) ac susceptibility components at different dc fields for **2**.

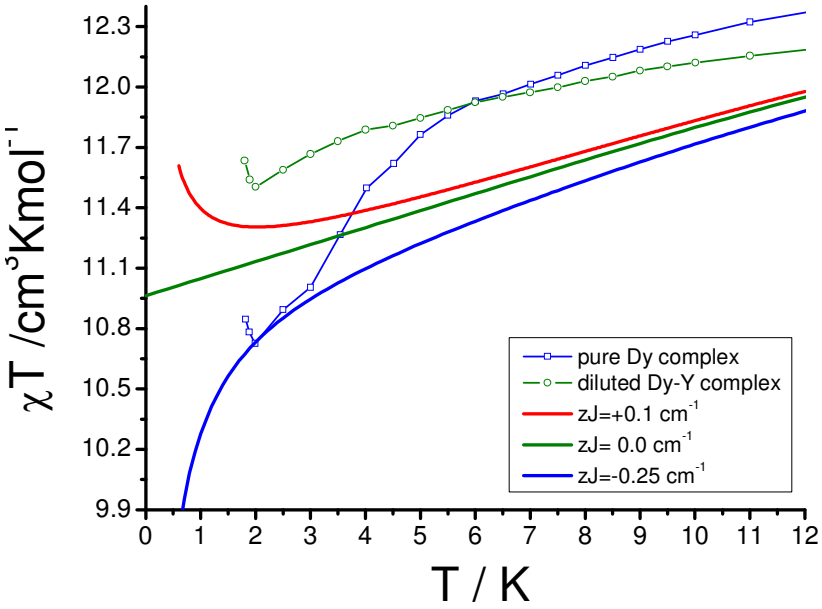

Figure S9. A zoom in the low temperature comparison between the measured magnetic susceptibility of the diluted Dy-Y and pure mononuclear Dy complex. The solid lines are the results of ab initio calculation of **1** with the basis **1-B** (see the main text) for the values of intermolecular interaction parameter indicated in the inset.

Ab initio calculations for Dy complex (1) and fragment *ab initio* calculations for $DyMn_2$ complex (2)

All employed basis sets were taken from the standard ANO-RCC (atomic natural orbitals with relativistic core correction) basis set library from MOLCAS. The following contractions were used for the atoms:

Dy – 8s7p5d4f2g1h.
La – 7s6p4d3f1g.
Mn – 7s6p4d3f2g1h.
Zn – 6s5p3d2f1g.
O – 4s3p2d1f. (only for the first coordinated atoms, which make a bond with Dy)
C – 4s3p1d. (only for the atoms which are directly bonded to the first coordination sphere of O)
N,O, C – 3s2p. (for distant atoms)
H – 2s. (for distant atoms)
Calculations based on the above basis sets are denoted **1-B** and **Dy from 2.**

For mononuclear Dy complex (**1**) we employed one more basis set approximation, **1-A**, which uses smaller basis sets on the atoms:

Dy – 7s6p4d3f1g.
N, O, C – 3s2p.
H – 2s.

Table S2. CASSCF and RASSI energies of the lowest spin-free states (cm^{-1}) on magnetic sites.

Spin multiplicity		**Spin free energies (CASSCF)**			**Spin-orbit energies (RASSI)**		
		1-A	**1-B**	**Dy from 2**	**1-A**	**1-B**	**Dy from 2**
6	H	0.000	0.000	0.000	0.000	0.000	0.000
		5.500	3.529	34.215	106.158	89.834	65.297
		182.724	141.436	90.582	166.896	152.825	102.239
		229.748	195.242	162.928	249.098	243.372	151.160
		240.708	203.546	205.824	374.863	362.444	166.898
		397.595	358.162	217.022	543.868	524.122	232.760
		454.949	445.095	238.932	726.157	691.944	271.592
		773.583	735.895	270.589	794.328	820.969	389.321
		781.850	755.509	350.912	3623.877	3602.517	3607.590
		888.657	895.117	509.830	3672.146	3666.631	3644.659
		901.528	900.985	535.637	3774.702	3767.934	3667.290
	F	7674.616	7647.234	7562.016	3858.552	3849.739	3690.545
		7777.117	7749.700	7608.688	3971.156	3955.361	3719.470
		7965.764	7923.811	7635.031	4112.493	4092.564	3748.107
		7971.060	7949.671	7683.454	4268.167	4269.184	3812.001
		7983.360	7972.694	7740.548	6198.232	6195.224	6166.778
		7990.479	7986.282	7794.448	6244.277	6257.689	6187.865
		8040.823	8012.124	7826.485	6327.873	6339.318	6216.197
	P	34897.345	34844.214	34908.844	6417.881	6430.371	6239.623
		34948.507	34927.681	34941.425	6543.614	6764.989	6318.481
		35837.961	35810.836	35129.948	6749.669	6764.989	6318.481
4		24972.045	24943.345	24870.045	8167.062	8164.637	8107.159
		24977.994	24949.774	24877.343	8234.369	8239.892	8134.479
		25029.624	24995.505	24898.231	8325.729	8342.052	8180.404
		25042.121	25004.613	24916.147	8433.187	8427.688	8224.591
		25119.618	25084.480	24932.947	8659.401	8673.031	8264.555
		25126.466	25105.642	24959.295	9686.603	9690.179	9642.154
		25137.670	25124.806	24968.034	9794.069	9812.615	9673.909
		25192.513	25147.391	25001.153	9920.925	9923.928	9736.418
		25199.435	25185.817	25003.339	10097.710	10088.398	9803.843
		25216.754	25190.544	25067.215	10163.193	10176.712	9989.212
		…	…	…	10214.755	10204.927	10011.386
2		37493.881	37453.847	37306.052	10281.666	10275.457	10048.373
		37496.427	37456.127	37310.486	10310.459	10299.824	10063.430
		37528.187	37488.538	37318.471	10345.681	10351.072	10107.699
		37530.908	37490.156	37332.638	10388.027	10383.622	10140.031
		37579.608	37536.872	37359.410	10806.526	10847.474	10835.102
		37600.176	37557.506	37365.610	11073.978	11109.712	10904.979
		37627.924	37589.683	37389.530	11369.452	11423.048	11018.991
		37632.581	37596.052	37447.997	11639.255	11688.833	11499.411
		37729.793	37694.580	37481.386	11653.415	11714.245	11542.240
		37743.658	37701.360	37483.900	11704.517	11768.444	11552.775
		…	…	…	…	…	…

Table S3. Energies of the lowest spin-free states and of the lowest spin-orbit Kramers doublets on manganese sites (cm^{-1}).

Spin multiplicity	Spin-free energies (CASSCF)		Spin-orbit energies (RASSI)	
	Mn1	**Mn2**	**Mn1**	**Mn2**
6	0.000	0.000	0.000	0.000
4	26811.813	26895.342	0.135	0.115
	27454.082	27577.310	0.221	0.199
	29147.064	29001.609	26802.760	26886.912
	30456.207	30433.062	26806.890	26890.426
	30651.816	30612.088	27445.380	27568.657
	30658.321	30657.805	27454.356	27576.397
	31008.283	31071.669	29135.957	28990.462
	31102.320	31110.345	29143.609	28998.312
	31173.186	31181.825	30438.816	30414.248
	36827.956	36960.092	30450.305	30426.742
	37390.100	37446.043	30623.218	30595.977
	37591.354	37628.302	30647.812	30615.205
	37828.476	37799.808	30671.068	30666.512
	38391.042	38468.868	30688.419	30675.101
	38808.634	38900.913	31005.706	31068.248
	…	…	31010.483	31072.830
2	38200.977	38179.183	31099.178	31107.315
	39922.653	39792.421	31102.939	31111.678
	40239.544	40285.955	31171.602	31180.703
	40698.890	40829.288	31176.292	31184.559
	41232.001	41361.586	36660.543	36788.297
	41534.820	41560.551	36756.073	36886.306
	41742.594	41799.148	37340.779	37367.945
	42295.363	42339.039	37392.676	37412.846
	43267.869	43139.040	37486.087	37532.021
	43372.078	43345.742	37615.844	37667.746
	43484.281	43440.041	37807.525	37799.321
	43645.046	43594.053	37921.200	37925.718
	44199.193	44234.932	38186.554	38167.445
	46155.078	46332.023	38349.929	38423.062
	46396.670	46622.447	38421.417	38509.257
	…	…	38764.652	38845.202
			38839.406	38922.739
			39221.971	39278.396
			…	…

Single_Aniso calculations of *g*-factors for Dy complex (1) and mononuclear fragments of $DyMn_2$ complex (2)

Table S4. Main values of the *g* tensor for the lowest Kramers doublets.

Kramers doublet		Main values of the g-tensor		
		1-A	**1-B**	**Dy from 2**
1	g_X	0.0238	0.0219	0.0682
	g_Y	0.0445	0.0729	0.1542
	g_Z	18.7688	18.7267	19.3367
2	g_X	0.6325	0.6954	0.7076
	g_Y	1.5260	1.5497	1.3635
	g_Z	13.6831	13.9892	18.3100
3	g_X	3.2459	2.4107	3.1590
	g_Y	4.4099	3.0916	4.1608
	g_Z	9.1422	10.2540	12.3346
4	g_X	3.9238	4.7687	0.1236
	g_Y	4.1988	5.5660	3.0691
	g_Z	8.2688	7.3321	13.8807
5	g_X	0.7064	1.2396	1.6454
	g_Y	1.0311	1.5153	4.2308
	g_Z	12.0131	11.6576	12.7762
6	g_X	0.2620	0.3198	0.1809
	g_Y	0.3503	0.3928	3.7347
	g_Z	14.9859	14.9759	10.4731
7	g_X	0.0161	0.0035	1.4462
	g_Y	0.0383	0.0112	2.8644
	g_Z	17.5421	18.5701	15.2401
8	g_X	0.0242	0.0071	0.0029
	g_Y	0.0461	0.0093	0.0169
	g_Z	19.4627	19.8037	19.0895

Table S5. Main values of the g-tensor for the ground $S = 5/2$.

		Main values of the g-tensor	
		Mn1	**Mn2**
1	g_X	2.0021	2.0021
	g_Y	2.0021	2.0021
	g_Z	2.0021	2.0021

Single_Aniso calculations of *magnetism* for Dy complex (1)

The difference between the calculated magnetic properties in computational models **1-A** and **1-B** is negligible. In the following the calculation of magnetism in **1** is reported for the basis set **1-B**.

As reported elsewhere (*Dalton Trans.* **2007**, *40*, 4582-4588), the position of hydrogen atoms connected to the firstly-coordinated atoms have an important effect on the energies of the low-lying states. Due to the uncertainty in the position of four H atoms for **1**, the obtained energies of the low-lying states are not accurate. However, a reduction of 50% of the energy on the first excited Kramers doublet leads to a much closer agreement with the experiment for all calculated magnetic properties.

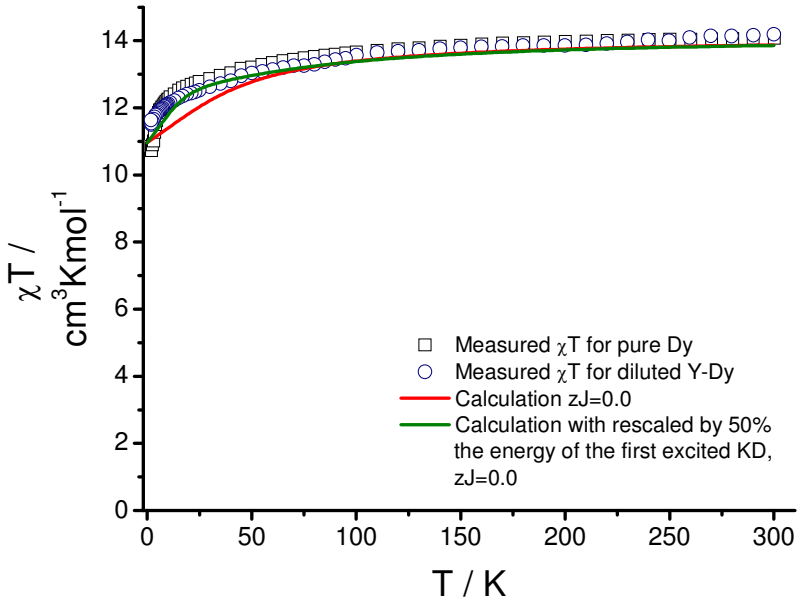

Figure S10. A comparison between measured magnetic susceptibility (empty figures) and calculated (red line) magnetic susceptibility for the complex **1** in computational model **1-B**.

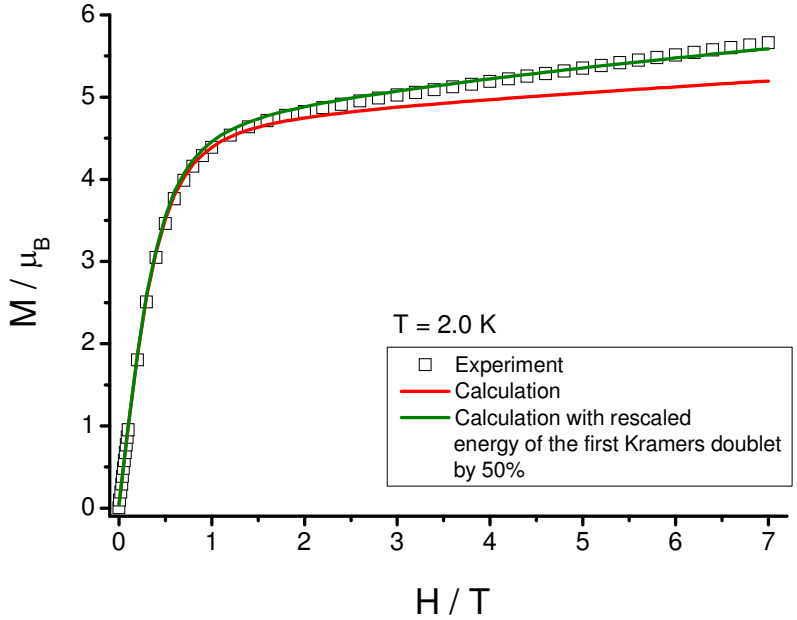

Figure S11. A comparison between measured (empty squares) and calculated (red line) molar magnetization at 2.0 K for the complex **1** in computational model **1-B**.

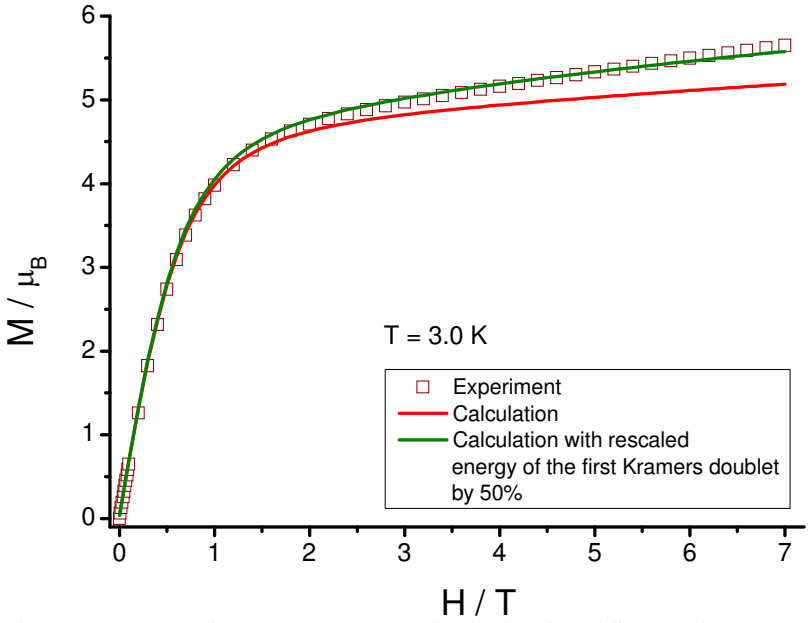

Figure S12. A comparison between measured (empty squares) and calculated (red line) molar magnetization at 3.0 K for the complex **1** in computational model **1-B**.

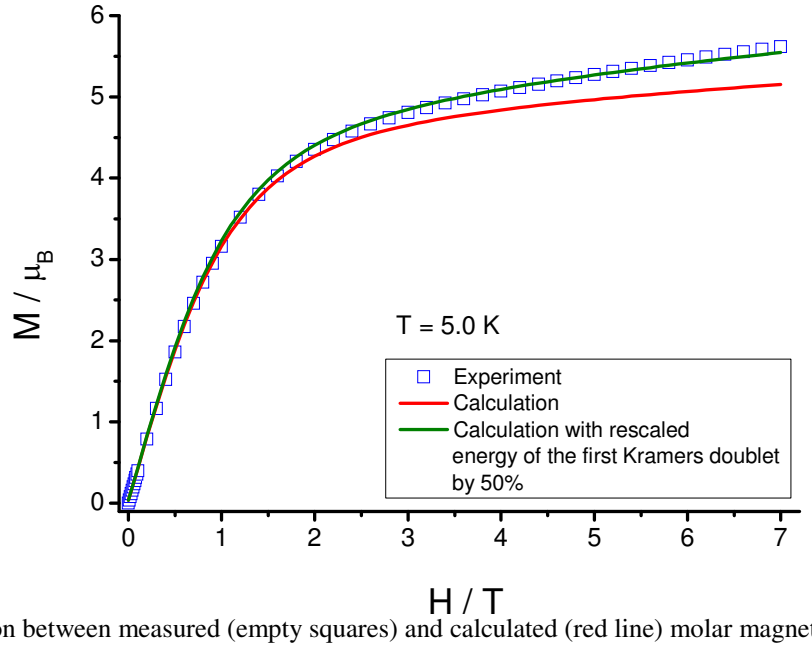

Figure S13. A comparison between measured (empty squares) and calculated (red line) molar magnetization at 5.0 K for the complex **1** in computational model **1-B**.

Exchange coupling and simulations of magnetism in $DyMn_2$ complex (2):

The following exchange interactions have been considered (see Eq. (1) from the main text):

J(Dy-Mn) = J_1
J(Mn1-Mn2)=J_2

The exchange interaction was considered within the Lines model (M. E. Lines, *J. Chem. Phys*. **1971**, *55*, 2977 – 2984.) and included the entire J=15/2 of the Dy^{3+} ion, and the ground S=5/2 of both Mn^{2+}. This results in a basis of 16 ×6×6=576 exchange functions. The molar magnetization was computed via a diagonalization of the Zeeman Hamiltonian in this basis. and adding the contributions from the Zeeman admixture of next excited multiplets on Dy center.

The least squares fit of the magnetic properties lead to the following Lines exchange coupling parameters:
First set: J_1= +0.044 cm^{-1} ; J_2= 0.000 cm^{-1}
Second set: J_1= +0.032 cm^{-1} ; J_2= +0.030 cm^{-1}

The exchange parameters with respect to effective S=1/2 on Dy^{3+} ion and S=5/2 on Mn^{2+} are:
First set: J_1= +0.22 cm^{-1} ; J_2= 0.000 cm^{-1}
Second set: J_1= +0.16 cm^{-1} ; J_2= +0.030 cm^{-1}

The difference between calculated magnetic properties using these sets of exchange parameters is negligible.

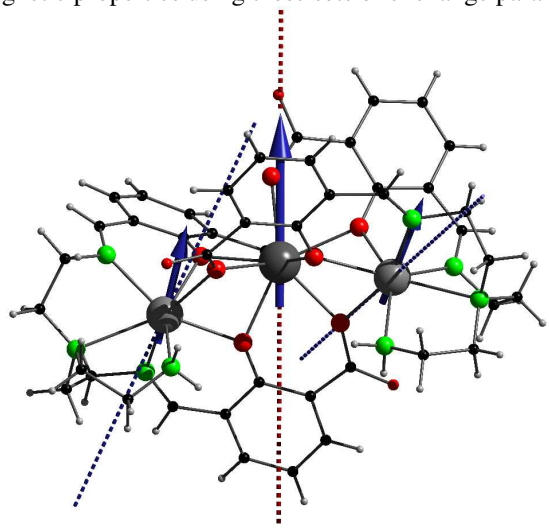

Figure S14. Anisotropy axes (dashed lines) and local magnetic moments (arrows) in the ground exchange state of **2**.

Table S6. Exchange energies (cm^{-1}) and main values of the *g* tensor for the 10 lowest exchange doublets.

Kramers doublet	***Second set:*** J_1= +0.16 cm^{-1} ; J_2= +0.030 cm^{-1}			***First set*:** J_1= +0.22 cm^{-1} ; J_2= 0.000 cm^{-1}		
	Energy (cm^{-1})	**Main values of the g-tensor**		**Energy (cm^{-1})**	**Main values of the g-tensor**	
1	0.000000 0.000000	g_X g_Y g_Z	0.000061 0.000085 37.968359	0.000000 0.000000	g_X g_Y g_Z	0.000048 0.000066 38.115700
2	0.136798 0.136798	g_X g_Y g_Z	0.002894 0.003754 35.224804	0.111885 0.111885	g_X g_Y g_Z	0.000555 0.000571 35.039610
3	0.237618 0.237618	g_X g_Y g_Z	0.030306 0.032501 31.573926	0.191777 0.191777	g_X g_Y g_Z	0.000573 0.001213 31.013959
4	0.317148 0.317148	g_X g_Y g_Z	0.042322 0.042911 32.930949	0.222468 0.222468	g_X g_Y g_Z	0.001807 0.002375 34.113041
5	0.346002 0.346002	g_X g_Y g_Z	0.167535 0.211475 28.613535	0.298151 0.298151	g_X g_Y g_Z	0.000544 0.001252 27.544306
6	0.390924 0.390925	g_X g_Y g_Z	0.093090 0.236568 28.651038	0.334320 0.334320	g_X g_Y g_Z	0.020456 0.020852 31.692736
7	0.431763 0.431764	g_X g_Y g_Z	0.173340 0.238438 24.855226	0.361673 0.361673	g_X g_Y g_Z	0.009303 0.011587 28.759460
8	0.467313 0.467313	g_X g_Y g_Z	0.035018 0.133504 25.621180	0.414201 0.414201	g_X g_Y g_Z	0.021665 0.044890 27.678504
9	0.492876 0.492876	g_X g_Y g_Z	0.100396 0.308564 21.065674	0.426344 0.426344	g_X g_Y g_Z	0.000272 0.000743 23.392838
10	0.551650 0.551650	g_X g_Y g_Z	0.019047 0.115059 25.737088	0.437173 0.437173	g_X g_Y g_Z	0.003189 0.007712 24.305743

Entire low-lying exchange splitting (2×6×6 = 72 states) of the complex **2** is 1.136 cm^{-1} for the first set of parameters and 1.203 cm^{-1} for the second set.

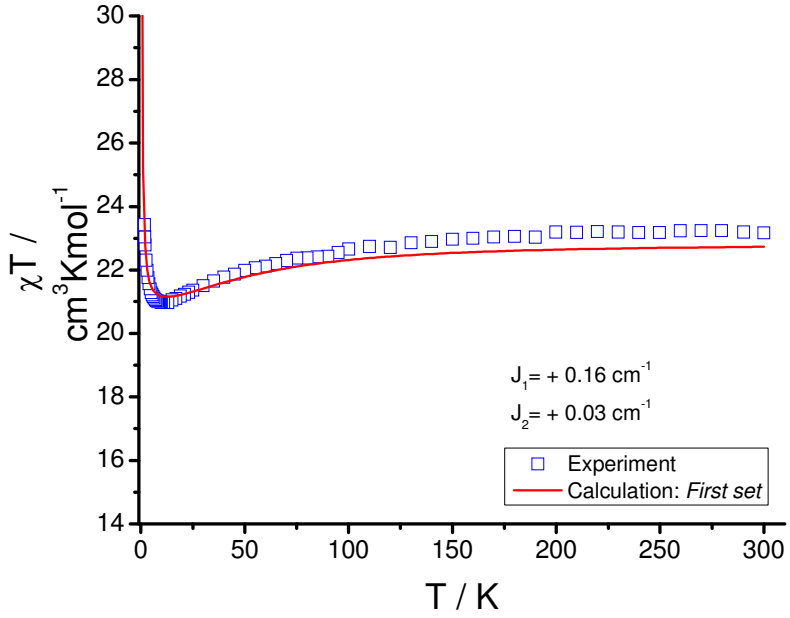

Figure S15. A comparison between measured magnetic susceptibility (empty figures) and calculated (red line) magnetic susceptibility for the complex **2**.

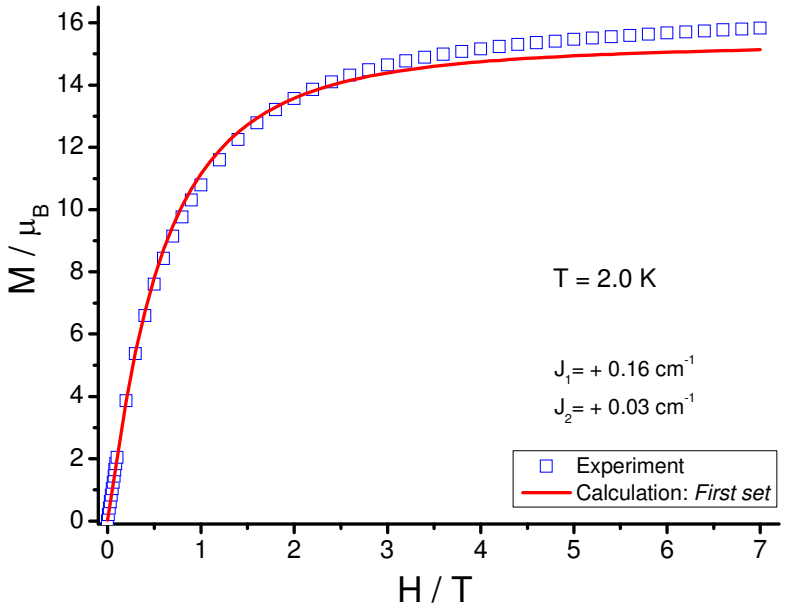

Figure S16. A comparison between measured (empty squares) and calculated (red line) molar magnetization at 2.0 K for the complex **2**.

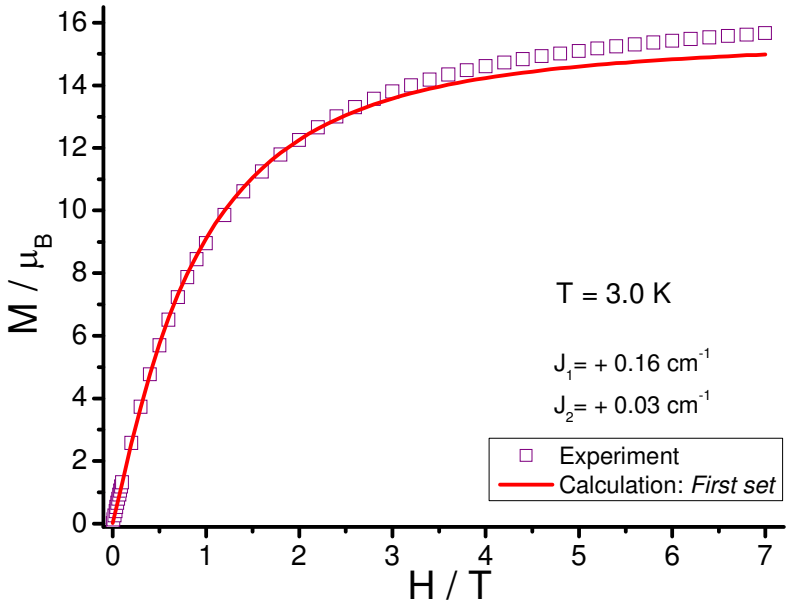

Figure S17. A comparison between measured (empty squares) and calculated (red line) molar magnetization at 3.0 K for the complex **2**.

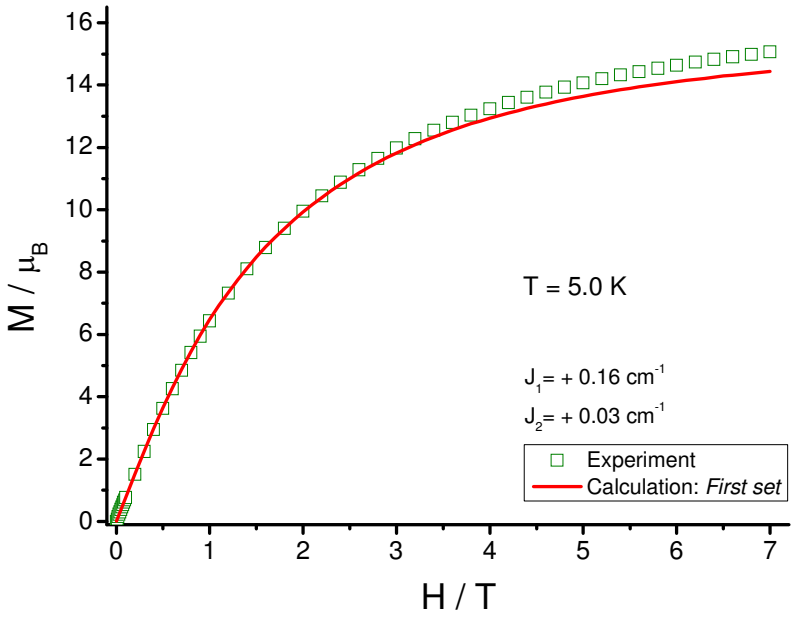

Figure S18. A comparison between measured (empty squares) and calculated (red line) molar magnetization at 5.0 K for the complex **2**.

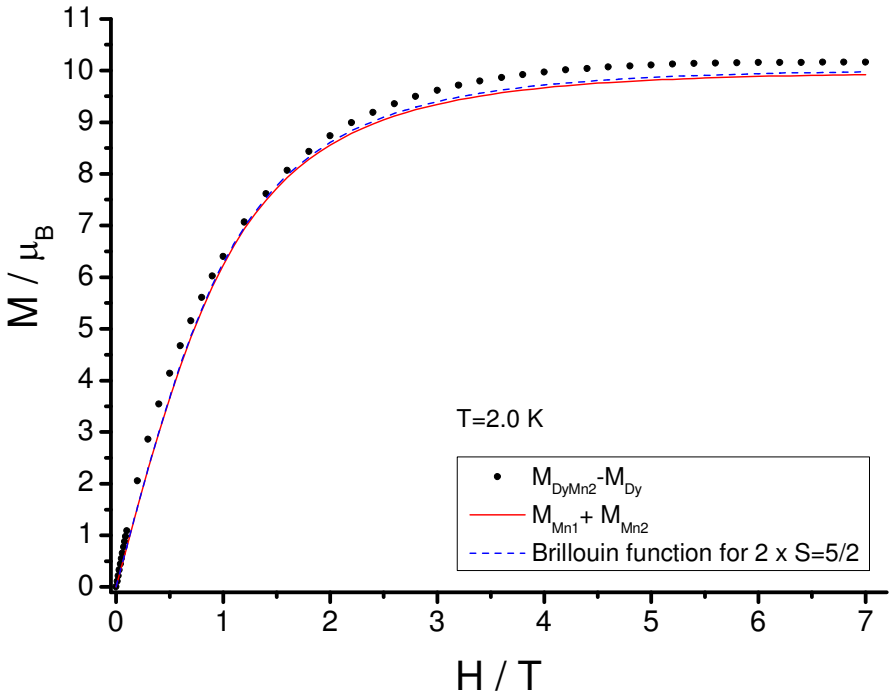

Figure S19: A comparison of field dependence of 'subtracted' magnetization (black circles) and the sum of individual contributions (calculated *ab initio*) from both Mn^{2+} ions (solid line). Dashed line show the sum of two Brillouin functions for S=5/2. The difference between the subtracted magnetization (M_{DyMn2}-M_{Dy}) and (M_{Mn1}+ M_{Mn2}) comes from the fact that the Dy ions in **1** and in **2** are different.

Estimation of the intermolecular interactions in 1.

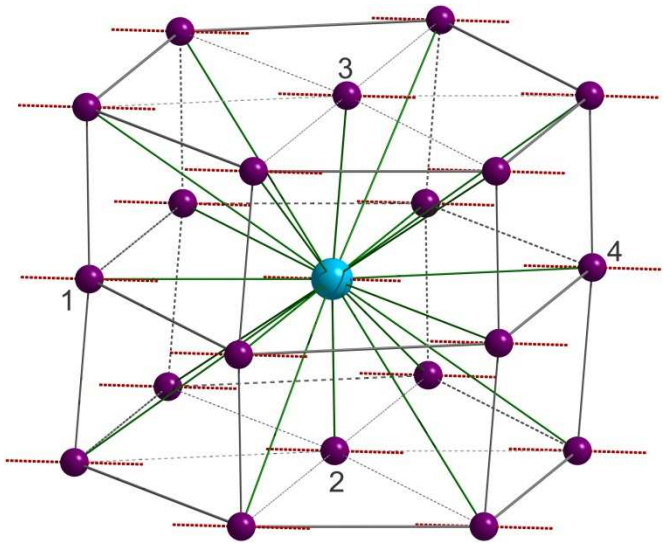

Figure S20. The nearest neighbor environment of 20 complexes (violet spheres) suroounding one chosen complex (blue sphere) in **1**.. Red dashed lines show the directions of local anisotropy axes calculated ab initio in the approximation **1-B** (see the main text). The numbers denote the complexes for which the dipolar interaction with the central complex are calculated in Table S7.

Table S7. Magnetic dipole interaction of Dy-Dy pairs specified in Figure S20.

Molecule No	$R_{Dy\text{-}Dy}$ (A)	$E_{Dy\text{-}Dy}$ (cm^{-1})	$J_{Dy\text{-}Dy}$ (cm^{-1})
1	12.482028297	-0.044853543	0.179414174
2	9.382268767	0.070793741	-0.283174964
3	9.915828737	0.054828348	-0.219313392
4	12.703777393	-0.049051866	0.196207465

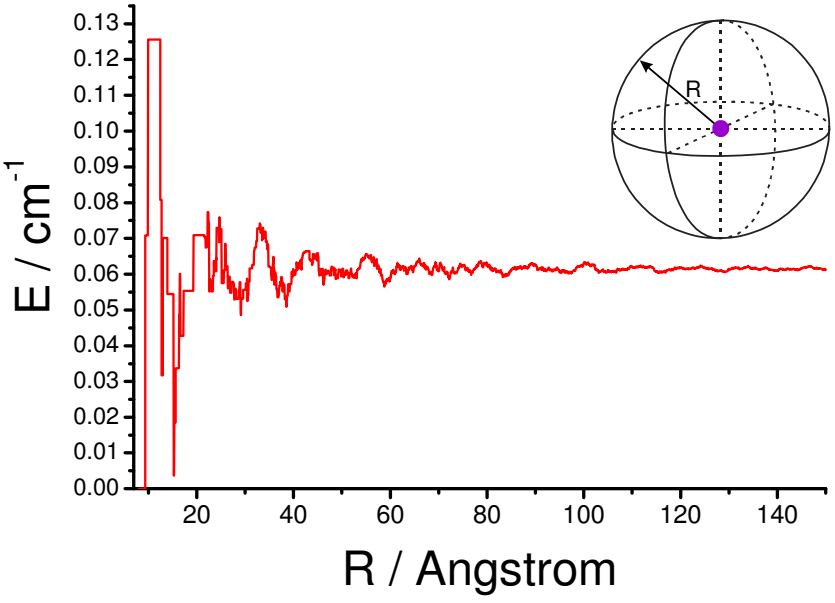

Figure S21. The same as Figure 3a for smaller maximal radius of the spherical sample **1**.

a)

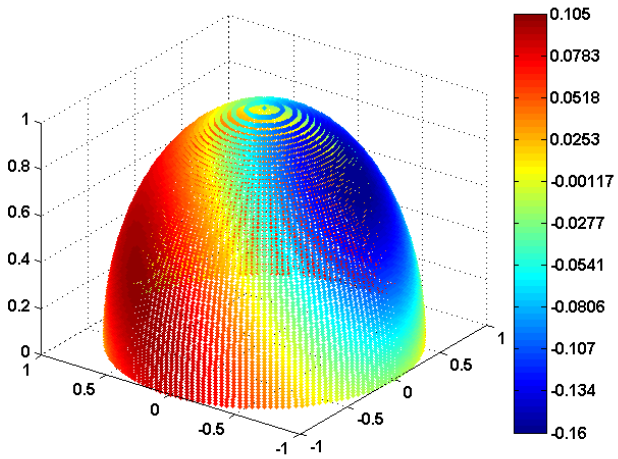

b)

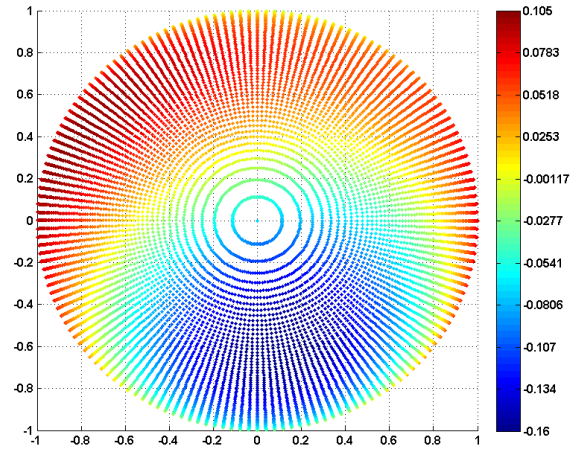

Figure S22. Dependence of the energy of intermolecular dipolar interaction of one central Dy complex with surrounding complexes in **1** in a large spherical sample (R>150Å) as function of the common direction of their anisotropy axes (position on the unit sphere). Plot (a) shows a three-dimensional view of the direction dependence of the amplitude of the interaction specified by colors. Plot (b) gives this view from the top. Only one hemisphere is shown, the second one gives an inverted distribution.

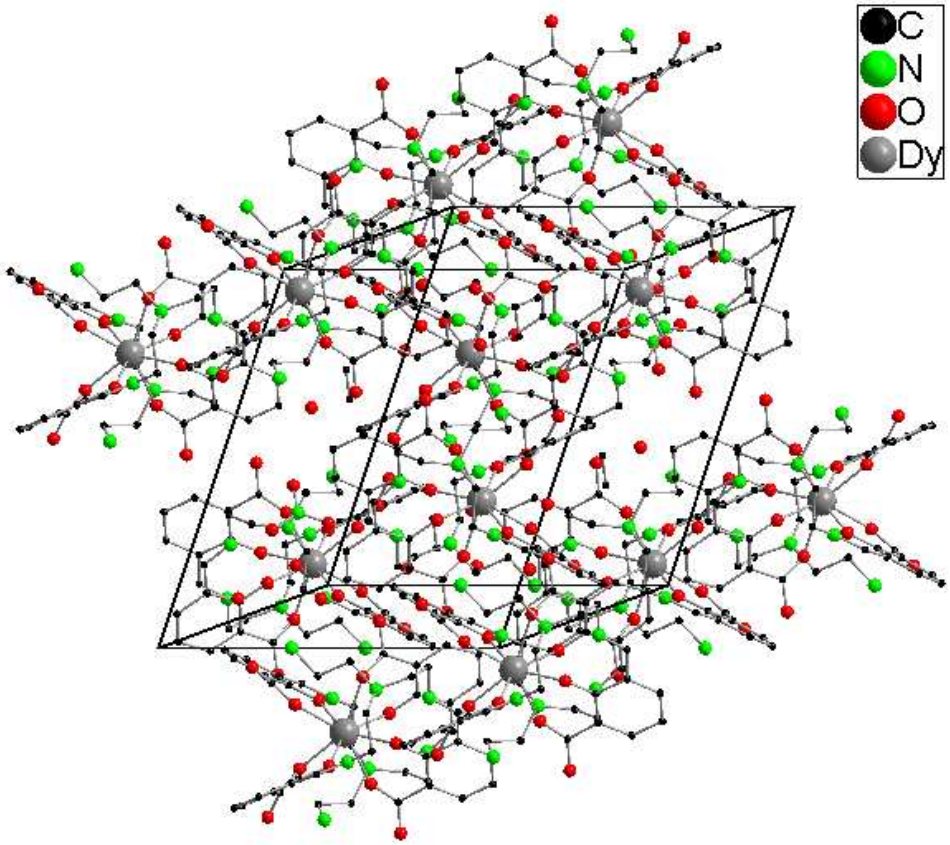

Figure S23: Cell Plot of compound **1** omitting the hydrogen atoms. View along the z-axis.

Supporting Information ESI-MS

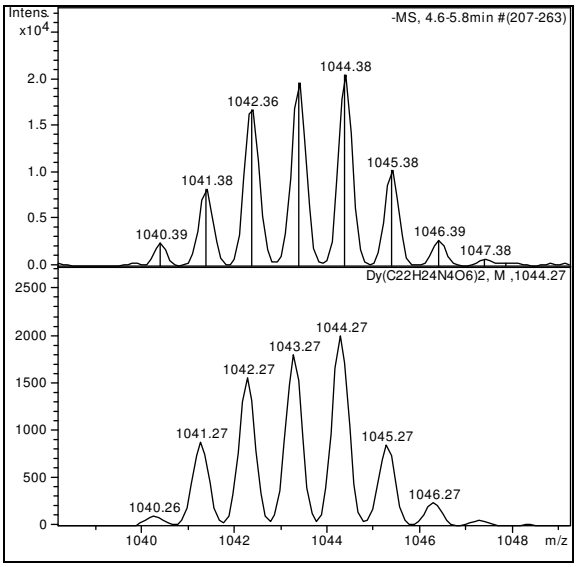

Fig. MS-S1a Top: experimental isotope pattern of $[Dy(H_2L)_2]^-$ (doubly deprotonated cation of compound **1**, $Dy(C_{22}H_{24}N_4O_6)_2$); bottom: simulation.

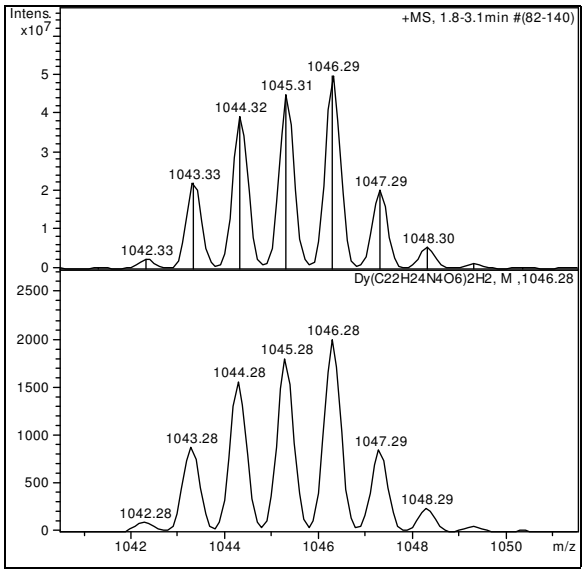

Fig. MS-S1b Top: experimental isotope pattern of $[Dy(H_3L)_2]^+$ (cation of compound **1**, $Dy(C_{22}H_{24}N_4O_6)_2H_2$); bottom: simulation.

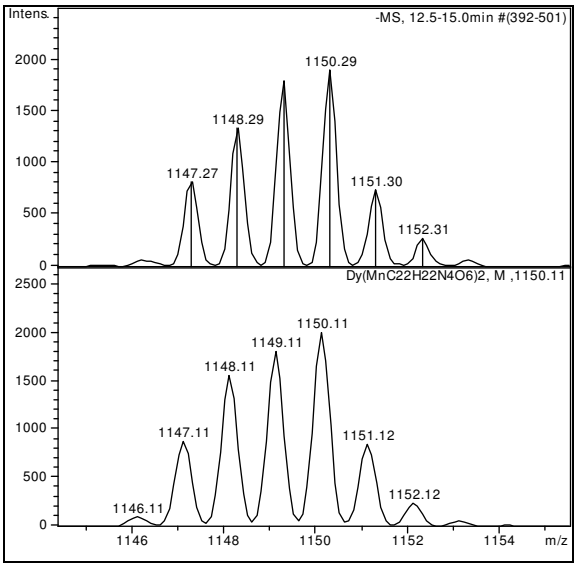

Fig. MS-S2a Top: experimental isotope pattern of $[Dy\{Mn(L)\}_2]^-$ (anion of compound **2**, $Dy(MnC_{22}H_{22}N_4O_6)_2$); bottom: simulation.

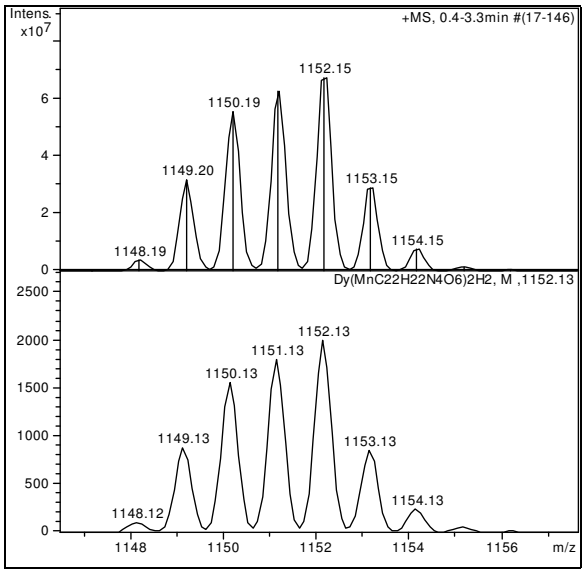

Fig. MS-S2b Top: experimental isotope pattern of $[Dy\{HMn(L)\}_2]^+$ (doubly protonated anion of compound **2**, $Dy(MnC_{22}H_{22}N_4O_6)_2H_2$); bottom: simulation.

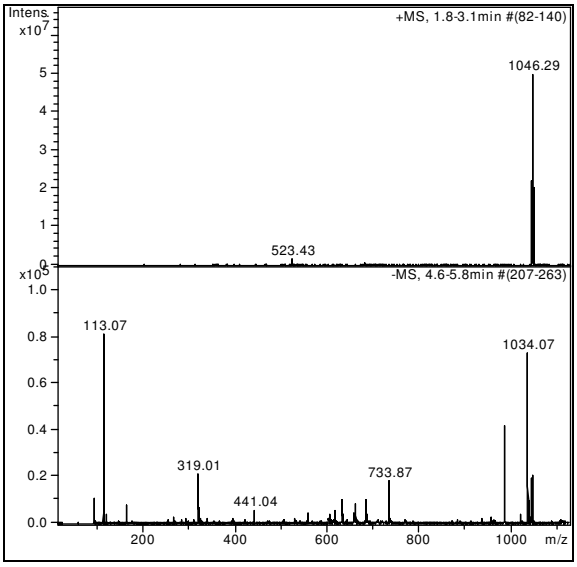

Fig. MS-S3 MS spectra of a solution of compound **1** in acetonitrile in positive (top) and negative (bottom) ion mode.

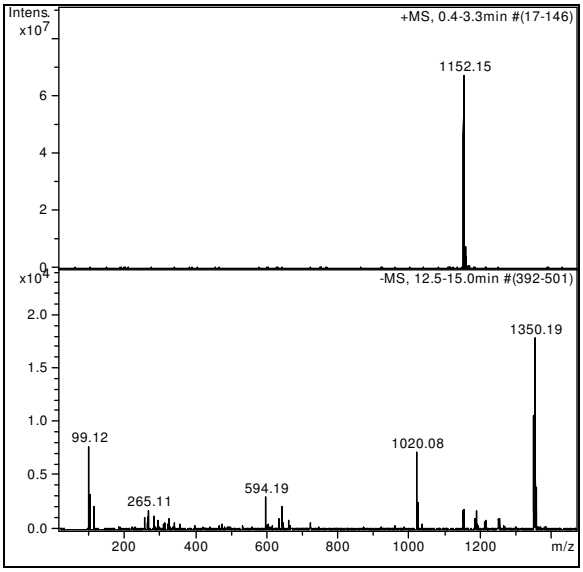

Fig. MS-S4 MS spectra of a solution of compound **2** in acetonitrile in positive (top) and negative (bottom) ion mode.

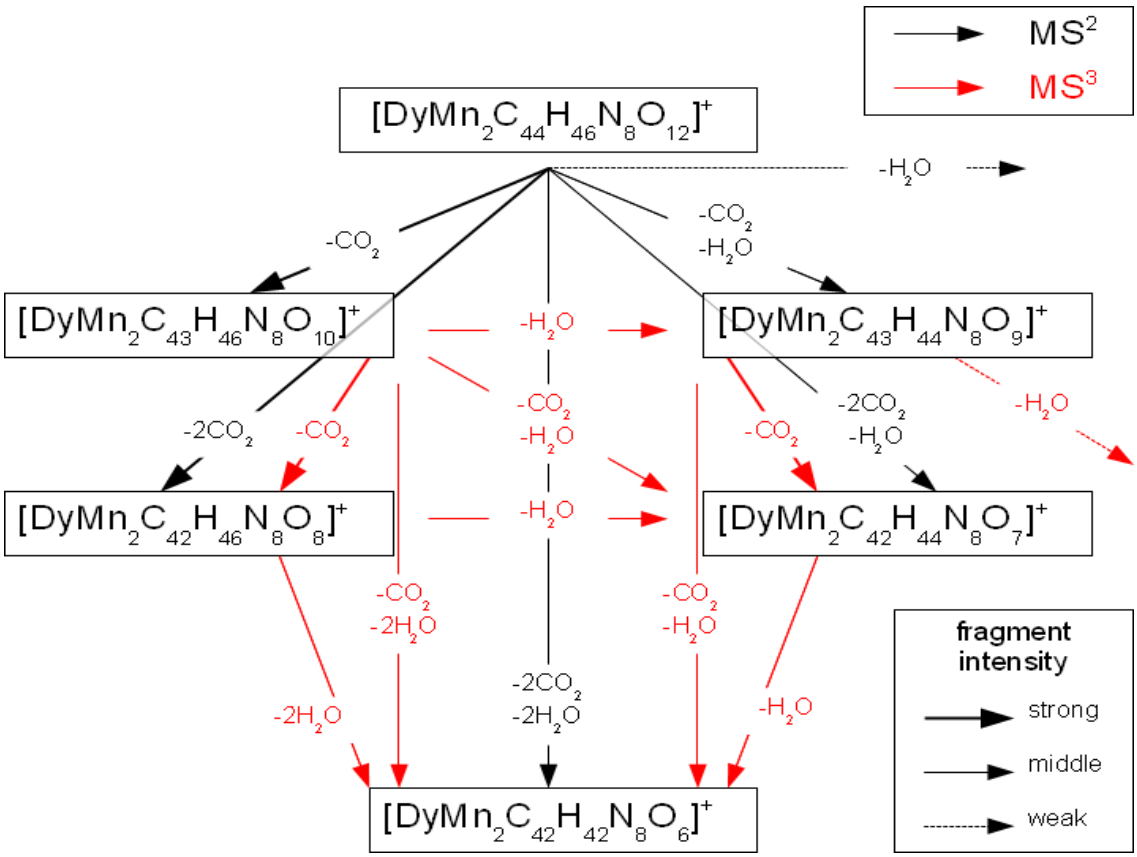

Scheme MS-S5 Fragmentation scheme of the neutral losses of CO_2 and H_2O from $[Dy\{HMn(L)\}_2]^+$.

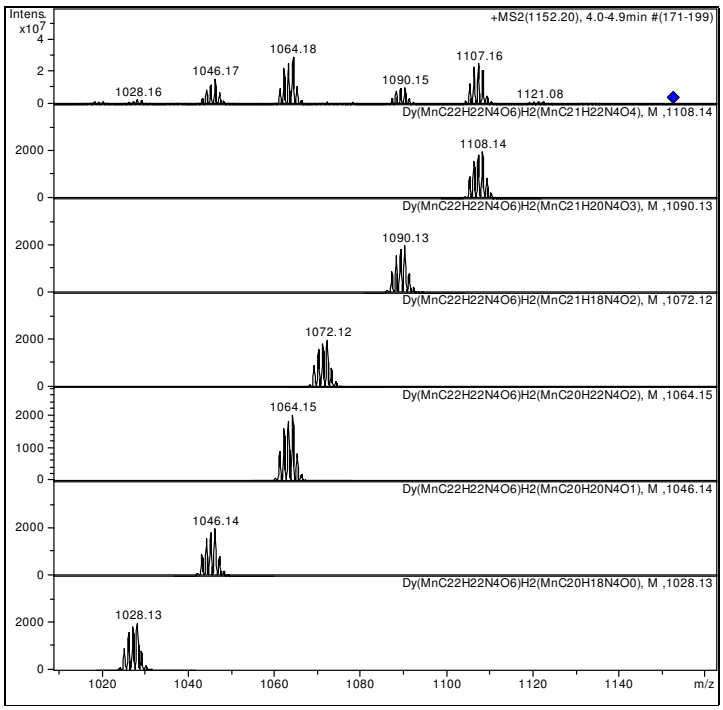

Fig. MS-S6 MS^n fragments (top) of $[Dy\{HMn(L)\}_2]^+$ and simulated mass peaks.

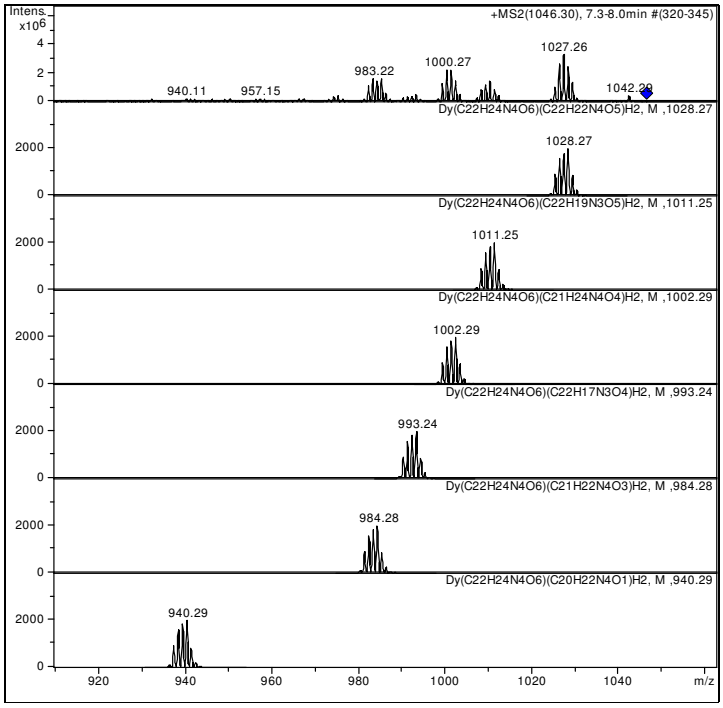

Fig. MS-S7 MS^n fragments (top) of $[Dy(H_3L)_2]^+$ and simulated mass peaks.

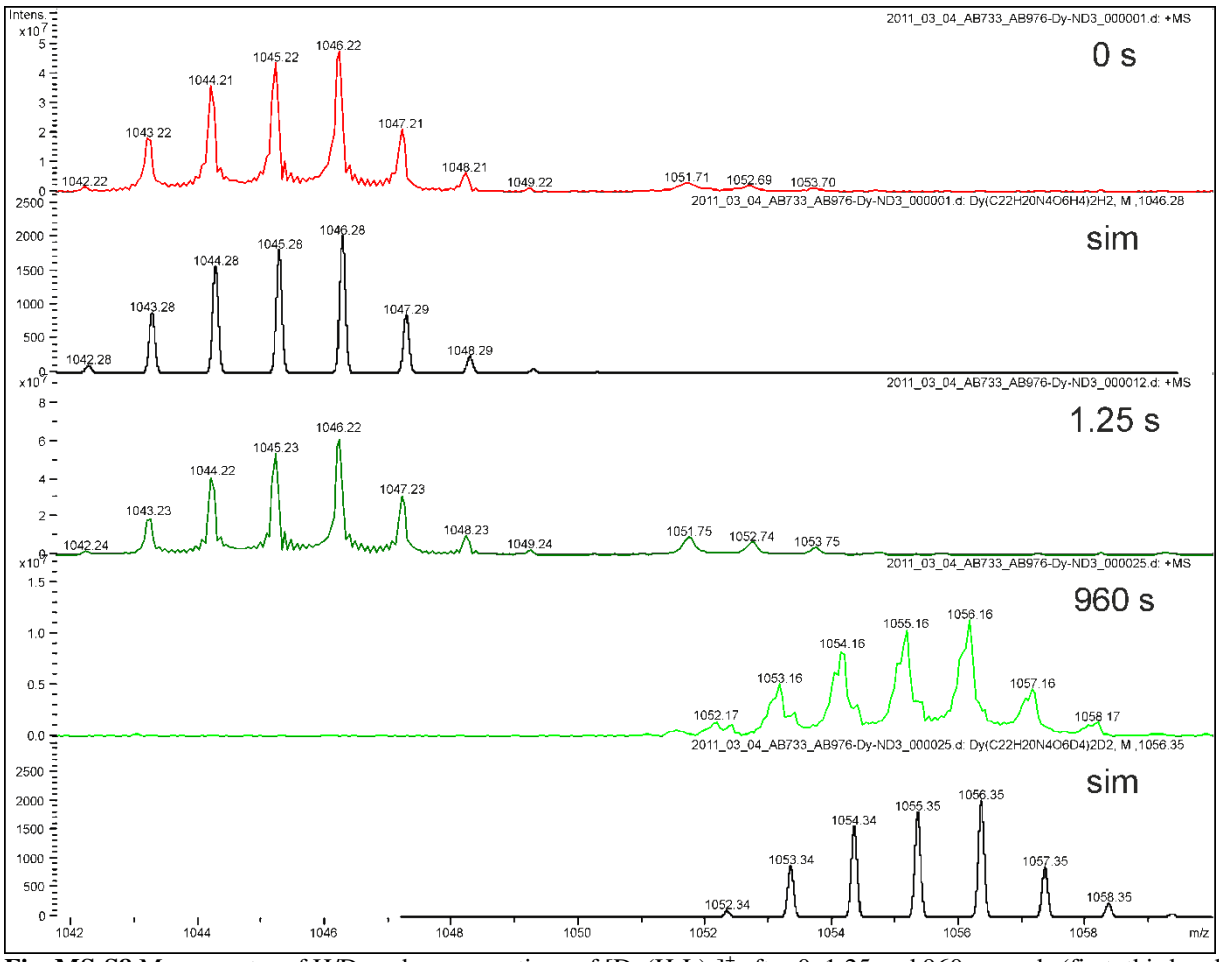

Fig. MS-S8 Mass spectra of H/D exchange reactions of $[Dy(H_3L)_2]^+$ after 0, 1.25 and 960 seconds (first, third and fourth row) and simulated isotope patterns (second and fifth row).

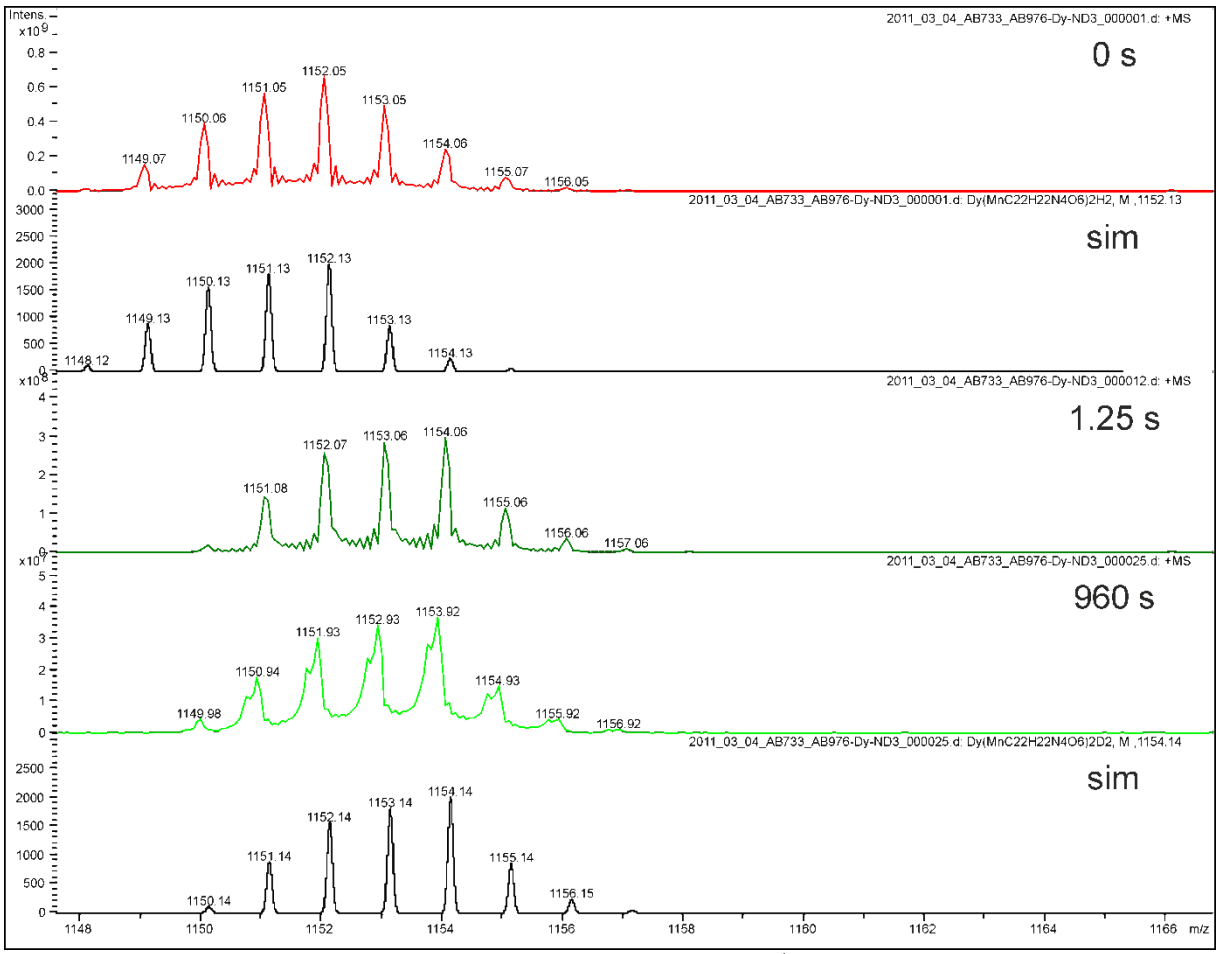

Fig. MS-S9 Mass spectra of H/D exchange reactions of $[Dy\{HMn(L)\}_2]^+$ after 0, 1.25 and 960 seconds (first, third and fourth row) and simulated isotope patterns (second and fifth row).